



**HAL**  
open science

# Resistive Load Influence on the Power and Bandwidth of Bistable Energy Harvesters

Quentin Demouron, Adrien Morel, David Gibus, Aya Benhemou, Adrien Badel

► **To cite this version:**

Quentin Demouron, Adrien Morel, David Gibus, Aya Benhemou, Adrien Badel. Resistive Load Influence on the Power and Bandwidth of Bistable Energy Harvesters. RTSI 2022 (7th Forum on Research and Technologies for Society and Industry Innovation), Aug 2022, Paris, France. pp.198-203, 10.1109/RTSI55261.2022.9905162 . hal-03764595

**HAL Id: hal-03764595**

**<https://hal.science/hal-03764595v1>**

Submitted on 30 Aug 2022

**HAL** is a multi-disciplinary open access archive for the deposit and dissemination of scientific research documents, whether they are published or not. The documents may come from teaching and research institutions in France or abroad, or from public or private research centers.

L'archive ouverte pluridisciplinaire **HAL**, est destinée au dépôt et à la diffusion de documents scientifiques de niveau recherche, publiés ou non, émanant des établissements d'enseignement et de recherche français ou étrangers, des laboratoires publics ou privés.

# Resistive Load Influence on the Power and Bandwidth of Bistable Energy Harvesters

Quentin Demouron

*Univ. Savoie Mont Blanc  
SYMME*

F-74000, Annecy, France

quentin.demouron@univ-smb.fr

Adrien Morel

*Univ. Savoie Mont Blanc  
SYMME*

F-74000, Annecy, France

adrien.morel@univ-smb.fr

David Gibus

*Univ. Savoie Mont Blanc  
SYMME*

F-74000, Annecy, France

david.gibus@univ-smb.fr

Aya Benhemou

*Univ. Savoie Mont Blanc  
SYMME*

F-74000, Annecy, France

aya.benhemou@univ-smb.fr

Adrien Badel

*Univ. Savoie Mont Blanc  
SYMME*

F-74000, Annecy, France

adrien.badel@univ-smb.fr

**Abstract**—Bistable piezoelectric energy harvesters are prominent solutions in the field of vibration energy harvesting due to their broadband behavior. However, the impact of the electrical interface and especially the load impedance needs to be addressed. In this study, the impact of the electrical load resistance on the dynamic of the bistable piezoelectric energy harvester has been studied. Through a parametric study, the present paper shows that the load resistance impacts both the harvested power and the bandwidth of the harvester. The analytical expression of the mass displacement, critical angular frequency and harvested power have been obtained, based on a truncated harmonic balance method. A comparison between the analytical model and experimental measurement on a custom bistable energy harvester is then presented. The experimental results are in good agreement with the analytical model, which proves the validity of the proposed model and analysis. The results presented in this study should be considered in the development of maximum power point tracking algorithms and orbit jump strategies.

**Keywords**—piezoelectricity, energy harvesting, nonlinear dynamical systems, electromechanical systems

## I. INTRODUCTION

During the last decades, there has been a growing interest for new energy harvesting solutions that could enable the development of battery-less sensors. Piezoelectric energy harvesters (PEH) are of particular interest because of their high energy density and their integration capability. PEH based on linear mechanical resonators [1] show interesting results provided that the vibration frequency matches the resonant frequency of the resonator. However, a slight mismatch of the vibration frequency leads to a drop of the harvested power. This constitutes a major issue in real applicative cases where both the vibration frequency and the PEH resonant frequency might vary with time [2]. To enlarge the bandwidth of PEH, researchers proposed to add nonlinearities to the mechanical resonator. Among the various nonlinear PEH that have been investigated in the literature, one of the most promising is the bistable PEH [3] [4].

Many research articles have focused on the mechanical optimization and analysis of bistable PEH. Erturk et al. [5] and Stanton et al. [6] demonstrated that bistable PEH exhibit high-power orbits that allow to considerably enlarge the bandwidth. In their work, Sneller et al. studied the impact of the inertial mass in order to optimize bistable PEH [7]. More recently, Liu et al. [8] and Saint-Martin et al. [9] proposed parametric

analysis of bistable PEH, describing the impact and influence of each parameter of bistable PEH.

Since PEH exhibit bidirectional electromechanical coupling, it has been proven that the electrical interface has a certain impact on the behavior of the system. Previous works focused on the load resistance impact on the bandwidth for linear piezoelectric energy harvesters [10] [11] and non-linear monostable piezoelectric energy harvesters [12]. The works presented in [13] focused on the load resistance optimization in order to maximize the harvested power for bistable PEH. However, to date and to the authors knowledge, no analytical and compact model of the impact of the load resistance on bistable PEH has been derived.

In this paper, we propose an analytical model with experimental validation of the load resistance impact on the harvested power as well as on the bandwidth of the system. First, we present the bistable PEH electromechanical model. In a second time, an analytical model of the electrical interface influence on the bistable dynamics is derived, by mean of a truncated harmonic balance. The experimental testbench and protocol are then presented. The experimental measurements are finally discussed and compared with the analytical model.

## II. ELECTROMECHANICAL MODEL OF BISTABLE PEH

### A. Bistable piezoelectric energy harvester

A piezoelectric energy harvester is a mechanical-to-electrical energy converter. It uses ambient vibrations as mechanical energy source. In this paper, we focus on a bistable piezoelectric energy harvester made of an inertial mass connected to two parallel buckled beams. The beams are clamped on one side and connected to an amplified piezoelectric actuator (APA) on the other side as depicted in Fig. 1. The APA is built around a stack of lead titano-zirconate piezoelectric ceramic (PZT) installed in an elliptical metallic shell.

When the beams are horizontal (which corresponds to an unstable position of the mass), the mass compresses the shell in its width, thereby stretching the piezoelectric ceramic stack and resulting in a negative voltage across the piezoelectric material. Conversely, when the mass reaches a positive (or negative) extremum, it stretches the shell in its width, thereby compressing the piezoelectric ceramic stack and resulting in a positive voltage across the piezoelectric material.

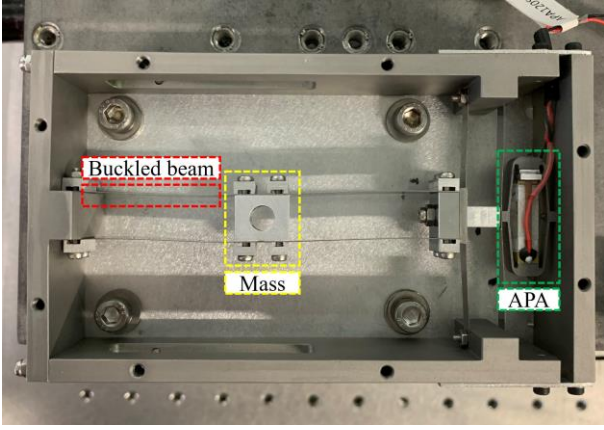


Fig. 1. Bistable piezoelectric energy harvester.

As detailed in [14], the differential equations modeling the electromechanical dynamic of the bistable piezoelectric energy harvester can be written as:

$$\begin{cases} \ddot{x} + \frac{\omega_0}{Q} \dot{x} + \frac{\omega_0^2}{2} \left( \frac{x^2}{x_0^2} - 1 \right) x + \frac{2\alpha}{ML} xv = \gamma(t) \\ C_0 \dot{v} = 2 \frac{\alpha}{L} x \dot{x} - \frac{1}{R} v \end{cases} \quad (1)$$

In (1),  $x$ ,  $x_0$ ,  $\alpha$  and  $v$  stand for the dynamic mass displacement, the “positive” equilibrium position of the mass, the force factor and the piezoelectric output voltage, respectively.  $M$ ,  $L$ ,  $R$  and  $C_0$  represent respectively the mass, the length of the buckled beams, the electrical load resistance and the capacitance of the piezoelectric material.  $Q$  and  $\omega_0$  stand for the mechanical quality factor and the natural resonant frequency of the equivalent linear resonator of the bistable, obtained for small displacements of the mass around one of its equilibrium positions.

Due to its bistability, the harvester may exhibit two families of orbits, known as intra-well and inter-well motions [9]. Intra-well motion consists in small oscillations of the inertial mass around one of the two stable positions  $x = \pm x_0$  whereas inter-well motion consists in oscillations around the two stable positions. Intra-well and inter-well motions can be defined respectively as low and high energy orbits.

### B. Analytical modelling

From (1), it can be seen that an electrical term  $\left(\frac{2\alpha}{ML} xv\right)$  is included in the mechanical equation. This electrical term can be associated with an electrically induced damping due to the electrical energy extracted from the harvester, as shown in [10] and [12] for instance. The first equation of (1) is reformulated to show the ratio between the electrical and the mechanical damping, noted  $\beta$ . Considering that the vibration is sinusoidal, the acceleration is expressed as:  $\gamma(t) = -\gamma_m \cos(\omega t)$ .

$$\ddot{x} + \frac{\omega_0}{Q} \dot{x}(1 + \beta) + \frac{\omega_0^2}{2} \left( \frac{x^2}{x_0^2} - 1 \right) x = \gamma(t) \quad (2)$$

The harmonic balance method is applied to (2) considering only the first harmonic of the mechanical displacement (higher order harmonics are not considered in the analytical expression). This approximation is reasonable since the waveform of the displacement is experimentally shown to be close to a sine wave. Considering that the system is at the

resonance ( $\omega = \omega_c$ ), a phase lag of  $90^\circ$  exists between  $x_m$  and  $\gamma$  as detailed in [15]. The resonance corresponds to the frequency for which the amplitude of the inter-well motion is maximal before this orbit suddenly disappears, therefore this frequency  $\omega_c$  is called *critical frequency* in the following. The expression of the inertial mass displacement at  $\omega = \omega_c$  can then be written as:  $x = x_m \sin(\omega t)$ . Applying harmonic balance on the first equation of (2) leads to:

$$\begin{aligned} & \cos(\omega t) \left[ -\gamma_m + \frac{\omega_0}{Q} \omega_c x_{m_c} + \frac{\omega_0 \beta}{Q} \omega_c x_{m_c} \right] \\ & + \sin(\omega t) \left[ -\omega_c^2 x_{m_c} + \frac{3\omega_0^2 x_{m_c}^3}{2x_0^2} - \frac{\omega_0^2}{2} x_{m_c} \right] = 0 \end{aligned} \quad (3)$$

From (3) the expression of the mass displacement amplitude  $x_{m_c}$  and the critical angular frequency  $\omega_c$  can be obtained by cancelling the factor terms of  $\sin(\omega t)$  and  $\cos(\omega t)$  respectively:

$$x_{m_c} = 2x_0 \sqrt{\frac{2}{3} \left( \frac{\omega_c^2}{\omega_0^2} + \frac{1}{2} \right)} \quad (4)$$

$$\omega_c = \sqrt{\frac{-\omega_0^2 + \sqrt{\omega_0^4 + \frac{6Q^2 \gamma^2}{x_0^2 (1 + \beta)^2}}}{4}} \quad (5)$$

From (5), the critical angular frequency depends on  $\beta$  and therefore on the electrical damping. Increasing the electrical damping implies the decrease of the critical angular frequency for which the high orbit disappears. Conversely, decreasing the electrical damping implies the increase of the critical angular frequency.

In the second equation of (1), the voltage frequency is considered twice greater than the excitation frequency. This is due to the fact that the piezoelectric element is constrained twice per cycle (one time for each equilibrium position). The piezoelectric voltage can therefore be expressed as:  $v = v_a \sin(2\omega t) + v_b \cos(2\omega t)$  where  $v_a$  and  $v_b$  stand for the in-phase and the out-of-phase components of the piezoelectric voltage. Applying the harmonic balance to the electrical equation of (1) leads to:

$$\begin{aligned} \frac{\alpha x_m^2 \omega \sin(2\omega t)}{L} &= 2\omega v_a C_0 \cos(2\omega t) - 2\omega v_b C_0 \sin(2\omega t) \\ &+ \frac{v_a}{R} \sin(2\omega t) + \frac{v_b}{R} \cos(2\omega t) \end{aligned} \quad (6)$$

Equation (6) leads to the expression of  $v_a$  and  $v_b$ :

$$\begin{cases} v_a = \frac{\alpha x_m^2 \omega R}{L + 4L\omega^2 C_0^2 R^2} \\ v_b = \frac{-2\alpha x_m^2 \omega^2 C_0 R^2}{L + 4L\omega^2 C_0^2 R^2} \end{cases} \quad (7)$$

From (7), we can express the piezoelectric output voltage:

$$\begin{aligned} v &= \frac{\alpha x_m^2 \omega R}{L + 4L\omega^2 C_0^2 R^2} \sin(2\omega t) \\ &- \frac{2\alpha x_m^2 \omega^2 C_0 R^2}{L + 4L\omega^2 C_0^2 R^2} \cos(2\omega t) \end{aligned} \quad (8)$$

Injecting (8) into the first equation of (1) leads to the expression of the electrical term of the mechanical equation:

$$\frac{2\alpha}{L} xv = \frac{2\alpha}{L} \left( \frac{v_a x_m}{2} (\cos(\omega t) - \cos(3\omega t)) + \frac{v_b x_m}{2} (\sin(3\omega t) - \sin(\omega t)) \right) \quad (9)$$

$\frac{2\alpha}{L} \left( \frac{v_a x_m}{2} \cos(\omega t) \right)$  corresponds to the voltage term in phase with the mechanical velocity at the resonant frequency ( $\dot{x} = x_m \omega_c \cos(\omega_c t)$ ). From this term yields the expression of the electrical damper:

$$\beta = \frac{x_m^2 k_m^2 Q}{x_0^2 4\Omega} \frac{r\Omega}{1 + 4(r\Omega)^2} \text{ with } \begin{cases} r = RC_0\omega_0 \\ \Omega = \frac{\omega}{\omega_0} \end{cases} \quad (10)$$

Where  $k_m^2$  stand for the electromechanical coupling coefficient. From (10), it can be seen that  $\beta$  depends on the load resistance. Moreover, there exists a value of the load resistance ( $r = \frac{1}{2\Omega}$ ) that maximizes the electrical damping. If the load resistance is smaller or larger than this value, the electrical damping is decreased.

The harvested power is estimated as the power dissipated in the resistive load  $R$  and is expressed as:

$$P_h = \frac{\beta \omega_0 M}{2Q} \dot{x}^2 \quad (11)$$

Injecting (4) in (11) leads to the expression of the harvested power and the maximum harvested power at the resonance:

$$P_h = \frac{4\beta M}{3} \frac{x_0^2 \omega^4}{Q \omega_0} \quad (12)$$

$$P_{h|\omega=\omega_c} = \frac{\gamma_m^2 \beta Q M}{2\omega_0(1+\beta)^2} \quad (13)$$

From (12) and (13), the harvested power depends on  $\beta$ . The harvested power reaches its maximum when  $\beta = 1$  which is the optimal value and means that the electrical damping is equal to the mechanical damping. Thus  $P_{h|\omega=\omega_c} = \frac{\gamma_m^2 Q M}{8\omega_0}$  and the harvested power decreases if  $\beta$  is smaller or larger than 1, which is a standard result for linear resonators.

Unless specified otherwise, the parameters that have been applied in order to compute Fig. 2 and Fig. 3 are presented in Table I. Fig. 2.a shows the harvested power as a function of the load resistance for three different values of the coupling coefficient. For a small coupling coefficient ( $k_m^2 = 1\%$ ), the harvested power is close to 3 mW and there exist only one value of the load resistance ( $R = \frac{1}{2C_p\omega}$ ) that maximizes the harvested power. Increasing the coupling coefficient (e.g.  $k_m^2 = 5\%$ ) allows to reach the power limit  $P_{h|\omega=\omega_c} = \frac{\gamma_m^2 Q M}{8\omega_0}$  and there exists two load resistances that are relatively close from each other and for which the harvested power reaches its maximum. For even higher coupling coefficient (e.g.  $k_m^2 = 20\%$ ), there exist two load resistances that maximize the harvested power. However, these two resistances are relatively spaced from each other compared to a smaller coupling coefficient. The critical frequency as a function of the load resistance for three different values of the coupling coefficient is illustrated in Fig. 2.b. For a small coupling coefficient ( $k_m^2 = 1\%$ ), the critical frequency is relatively high ( $f_c = 74.85$  Hz) whereas a larger coupling coefficient

( $k_m^2 = 20\%$ ) induces a relatively low critical frequency ( $f_c = 32.38$  Hz). Increasing the coupling coefficient implies the increase of the electrical damping, thus resulting in the decrease of the critical frequency. Moreover Fig. 2.b shows that the resistance which maximizes the electrical damping ( $R = \frac{1}{2C_p\omega}$ ) is conversely proportional to the critical frequency. Increasing the coupling coefficient implies the decrease of the critical frequency, thus increasing the load resistance for which the damping is maximal. The electrical damping as a function of the load resistance for three different values of the coupling coefficient is illustrated in Fig. 2.c. As shown in (10), a larger coupling coefficient induces the increase of the damping ratio  $\beta$ . If the coupling coefficient is larger than a certain value ( $k_m^2 > \frac{16\Omega x_0^2}{x_m^2 Q}$ ) there exists two load resistances allowing to reach  $\beta = 1$  and maximizing the harvested power. The bifurcation of the optimal resistance is similar to the one encountered in linear PEH [10].

Fig. 3.a illustrates the harvested power as a function of the frequency for both the bistable and the equivalent linear harvester (which corresponds to small oscillations of the mass around one of the two stable positions). The bandwidth is computed at half of the maximum harvested power. The equivalent linear harvester, exhibits a narrow bandwidth (1.88 Hz) and the harvested power reaches its maximum for a frequency equal to the resonant frequency of the system. This result can be obtained only with a perfect optimization of the damping ratio  $\beta$ . This optimization of the linear harvester is quite complicated to perform due to the large values of  $\beta$  that are required away from the resonant frequency (much larger than for the bistable PEH).

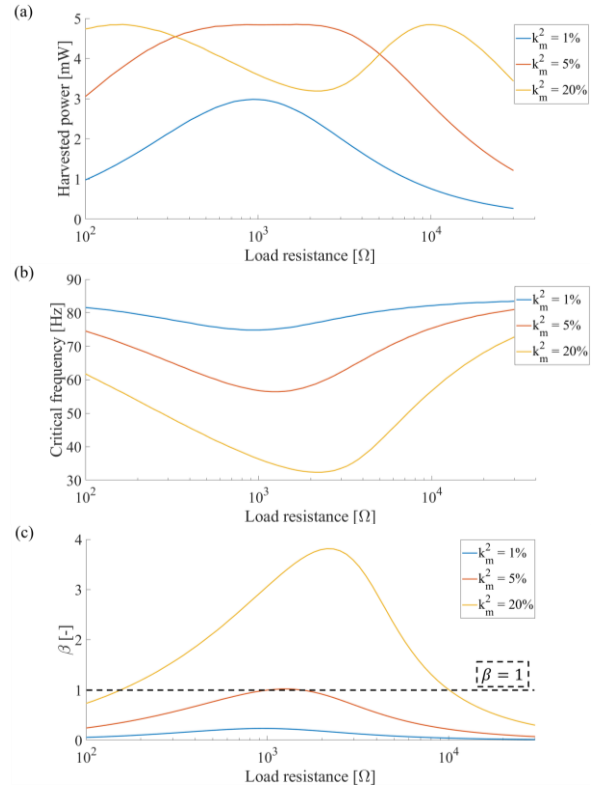


Fig. 2. (a) power, (b) critical frequency and (c)  $\beta$  as a function of the load resistance for three different coupling coefficient.

TABLE I. PROTOTYPE PARAMETERS

Experimental parameters		
Parameter	Value	Unit
Acceleration amplitude	5	$m \cdot s^{-2}$
Piezoelectric capacitance	$1.232e^{-6}$	F
Natural resonant frequency	335	$rad \cdot s^{-1}$
Dynamic mass	6.5	g
Buckled beam length	35	mm
Mechanical quality factor	80	—
Coupling coefficient	0.068	—

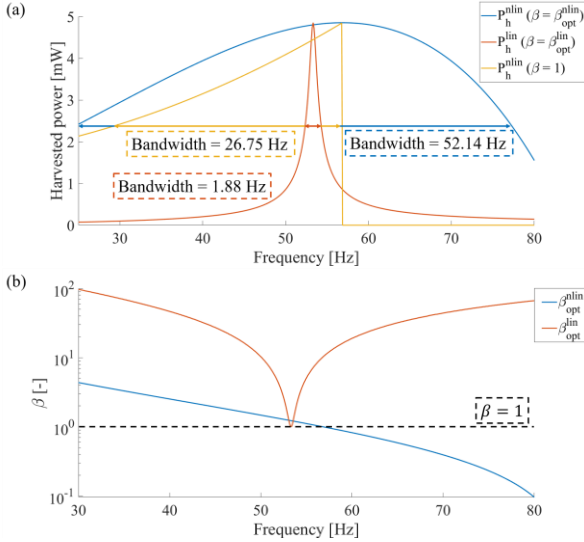


Fig. 3. (a) harvested power and (b) optimal electrical damping for the linear (orange) and the non-linear (blue and yellow) model.

The bistable harvester with  $\beta = 1$  (no optimization of  $\beta$  as a function of the frequency), exhibits a broader bandwidth (26.75 Hz) and the harvested power reaches its maximum when the frequency is equal to the critical frequency of the high orbit. Tuning the electrical damping of the bistable harvester ( $\beta = \beta_{opt}^{lin}$ ) allows to reach an even broader bandwidth (52.14 Hz). Fig. 3.b shows the optimal damping ratio for the bistable and the equivalent linear harvesters. In both cases, the harvested power reaches its maximum (4.85 mW) for  $\beta = 1$ . Note that in the case of bistable PEH, the optimal values of  $\beta$  are smaller than 1 for frequencies higher than the critical frequency.

### III. EXPERIMENTAL VALIDATION

#### A. Experimental testbench

An experimental testbench, depicted in Fig. 4, including a dSpace real time interface, an electromagnetic shaker and its associated power amplifier, a differential laser vibrometer and a programmable decade box has been set up. The piezoelectric energy harvester illustrated in Fig. 1 is fixed to the shaker. Note, that the characteristics of the prototype have been experimentally identified and are the same as the parameters used in section II (Table I). The shaker is driven in closed loop through the dSpace interface to control the amplitude of the sinusoidal excitation. Matlab scripts allow to modify the amplitude and the frequency of the excitation as well as the load resistance value. A differential laser vibrometer is used to measure the displacement and speed of the mass of the electromechanical harvester.

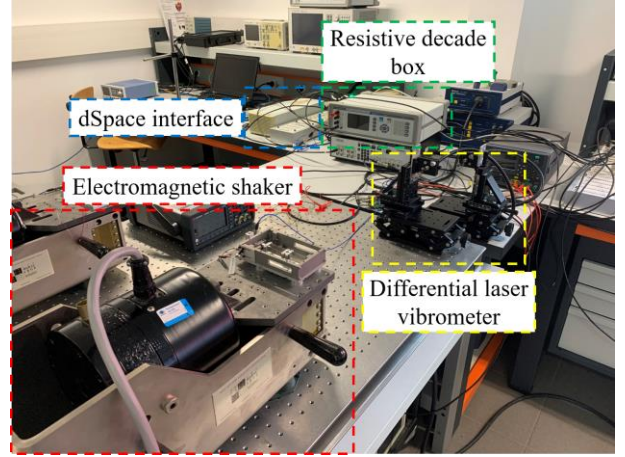


Fig. 4. Experimental testbench.

The piezoelectric output voltage is transferred to the dSpace interface by mean of a voltage follower in order to isolate the amplified piezoelectric actuator from the dSpace interface input impedance. Data acquisition is done with the dSpace interface. The displacement and the speed of the mass as well as the input acceleration and the piezoelectric output voltage are recorded.

#### B. Experimental protocol

As presented in the first part of this paper, the bistable piezoelectric energy harvester might exhibit two types of motion: intra-well and inter-well motions. The experimental characterization is performed on the inter-well motion also known as high-energy orbit. The PEH is submitted to a sinusoidal acceleration of amplitude  $\gamma_m = 5 m \cdot s^{-2}$  and the vibration frequency is swept from 30 Hz to 120 Hz. In order to force the inter-well motion operation of the energy harvester, an orbit jump sequence has been developed. At 44 Hz, the acceleration amplitude is progressively increased up to  $17 m \cdot s^{-2}$ . Under such large vibration amplitude, the energy harvester starts operating in inter-well motion. Finally, the acceleration amplitude is slowly decreased to  $\gamma_m = 5 m \cdot s^{-2}$  so that the harvester remains in inter-well operation even though the acceleration amplitude is smaller. The frequency is then swept up and down to cover the 30 Hz to 120 Hz frequency range.

The experimental parameters that have been applied in order to characterize the PEH are presented in Table II. The aforementioned orbit jump sequence and frequency sweep are performed for 70 load resistances (from 100  $\Omega$  to 30 k $\Omega$ ) as indicated in Table II. The voltage, displacement, speed and acceleration waveforms are stored for each combination of resistance and vibration frequency.

#### C. Experimental validation of the proposed model

To validate the analytical model, we compared the results obtained through analytical calculations and the results obtained through experimental tests for the set of parameters shown in Table II. We also ran numerical simulations in order to numerically solve (1) with the parameters shown in Table II. Results for the inertial mass displacement are presented in Fig. 5.a. For the central resistance  $R = 1409 \Omega$  the analytical model predicted a maximum displacement at the resonance (4)  $x_{m_c} = 1.5 mm$  which is in good agreement with the one obtained with numerical simulations and the measured displacement (respectively 1.56 mm and 1.59 mm).

TABLE II. EXPERIMENTAL PARAMETERS

Experimental parameters		
Parameter	Value	Unit
Acceleration amplitude	5	$m \cdot s^{-2}$
Frequency	30 – 120	Hz
Number of tested frequencies	910	–
Load resistance	100 – 30 000	$\Omega$
Number of tested load resistances	70	–

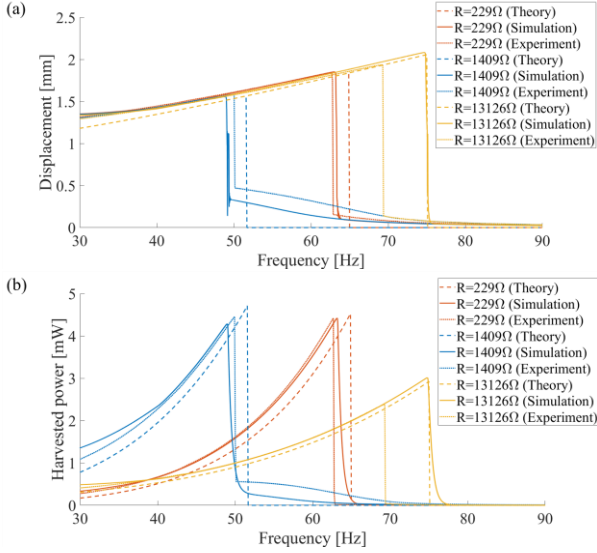


Fig. 5. (a) displacement and (b) harvested power for  $R = 229 \Omega$  (orange),  $R = 1409 \Omega$  (blue) and  $R = 13126 \Omega$  (yellow) in theory (dash), simulation (solid) and experiment (dot).

For frequencies smaller than the resonant frequency, the inertial mass displacement is also well predicted. For each of the analytical, simulated and experimental results, the slope of the inter-well orbit amplitude is almost identical. Regarding the critical frequency, a slight difference can be observed. This difference increases as the displacement amplitude increases which is due to mechanical nonlinearities (the higher the displacement, the lower the mechanical quality factor). For the central resistance the analytical model predicted a critical frequency  $f_c = 51.57 \text{ Hz}$  whereas the simulation and the experiment critical frequencies are smaller (respectively  $48.83 \text{ Hz}$  and  $49.93 \text{ Hz}$ ). Fig. 5.b shows the results for the harvested power. For the central resistance  $R = 1409 \Omega$ , the analytical model predicted a maximum harvested power at the resonance (13)  $P_h|_{\omega=\omega_c} = 4.7 \text{ mW}$  which is in good agreement with the one observed in simulation and experimental tests (respectively  $4.3 \text{ mW}$  and  $4.5 \text{ mW}$ ). For frequencies smaller than the resonant frequency, the harvested power (12) is also well predicted. The harvested powers with analytical, simulated and experimental results are relatively close.

#### D. Experimental results and discussion

Fig. 6 illustrates the experimental impact of the load resistance on the dynamic of the bistable PEH. The critical frequency of the inter-well motion  $f_c$  is a function of the resistance. For small resistance values ( $R < 200 \Omega$ ) or large resistance values ( $R > 20 \text{ k}\Omega$ ), this critical frequency is close to  $70 \text{ Hz}$ .

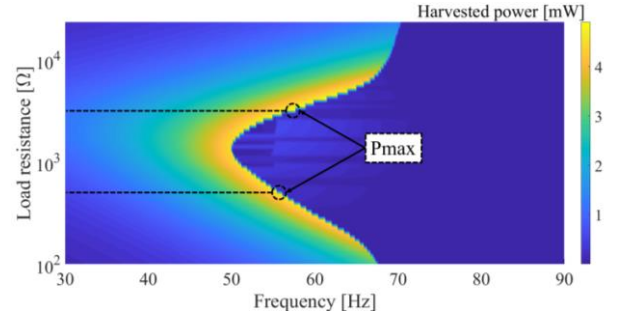


Fig. 6. Harvested power as a function of the frequency and the load resistance.

However, we can observe that  $f_c$  decreases until it reaches a minimum of  $50 \text{ Hz}$  when the resistance is close to  $1409 \Omega$ . Indeed, this resistance is equal to  $R = \frac{1}{2C_p\omega}$  (with  $C_p$  being the capacitance of the piezoelectric material and  $\omega = 314.15 \text{ rad}\cdot\text{s}^{-1}$  the angular frequency of the vibration) which maximizes the electrical damping. The harvested power depends on the electrical damping associated to the resistance value. Fig. 7.a illustrates that the harvested power reaches two maxima for two resistances ( $R = 522 \Omega$  and  $R = 3220 \Omega$ ). These two resistances allow to reach an electrical damping equal to the mechanical damping, thus maximizing the harvested power. If the resistance is close to  $1409 \Omega$ , the electrical damping is greater than the mechanical damping ( $\beta = 1.59$ ). The system is therefore overdamped and the harvested power slightly decreases. Conversely, if the resistance is larger than  $3220 \Omega$  or smaller than  $522 \Omega$ , the electrical damping is smaller than the mechanical damping ( $\beta < 1$ ) which explains that the harvested power also decreases.

These experimental results prove that it is possible to adjust the harvested power and the critical frequency by tuning the load resistance.

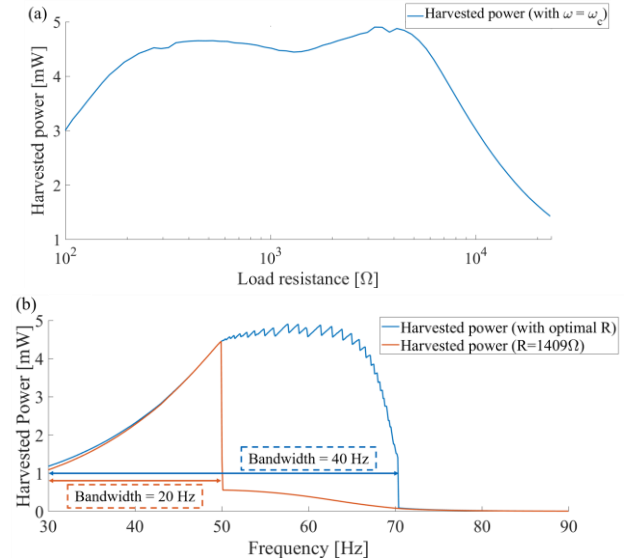


Fig. 7. (a) harvested power as a function of the load resistance for the critical frequency, (b) maximum harvested power (blue line) and harvested power for the maximum electrical damping (orange line) as a function of the frequency.

If the resistance is finely tuned for each vibration frequency, it is possible to harvest more than 1 *mW* over a frequency band from 30 *Hz* to 70 *Hz* as illustrated in Fig. 7.b. This result demonstrates the wideband behavior of the bistable harvester as well as the interest of designing adaptative electrical interfaces for which the input impedance is dynamically optimized as a function of the vibration.

#### IV. CONCLUSION

In this study, the impact of the electrical load resistance on the dynamic of a bistable piezoelectric energy harvester was investigated. It was shown that the load resistance not only impacts the harvested power but also has an impact on the mechanical behavior of the system and specifically on its bandwidth due to the damping induced by the electrical interface. Analytical modelling, simulation and experiments are in good agreement. The proposed analytical model allows to quickly estimate the bandwidth of the harvester as well as the harvested power. Moreover, these results should be considered in the development of maximum power point tracking algorithms and orbit jump strategies.

#### ACKNOWLEDGMENT

This work has been supported by the French government, under the Future Investment Program (Programme d'investissements d'avenir).

#### REFERENCES

- [1] J. Siang, M. H. Lim, et M. Salman Leong, « Review of vibration-based energy harvesting technology: Mechanism and architectural approach », *Int J Energy Res*, vol. 42, n° 5, p. 1866-1893, avr. 2018, doi: 10.1002/er.3986.
- [2] A. Morel, A. Badel, Y. Wandroild, et G. Pillonnet, « A unified N-SECE strategy for highly coupled piezoelectric energy scavengers », *Smart Mater. Struct.*, vol. 27, n° 8, p. 084002, août 2018, doi: 10.1088/1361-665X/aac3b6.
- [3] S. P. Pellegrini, N. Tolou, M. Schenk, et J. L. Herder, « Bistable vibration energy harvesters: A review », *Journal of Intelligent Material Systems and Structures*, vol. 24, n° 11, p. 1303-1312, juill. 2013, doi: 10.1177/1045389X12444940.
- [4] S. M. Shahruz, « Increasing the Efficiency of Energy Scavengers by Magnets », *Journal of Computational and Nonlinear Dynamics*, vol. 3, n° 4, p. 041001, oct. 2008, doi: 10.1115/1.2960486.
- [5] A. Erturk et D. J. Inman, « Broadband piezoelectric power generation on high-energy orbits of the bistable Duffing oscillator with electromechanical coupling », *Journal of Sound and Vibration*, vol. 330, n° 10, p. 2339-2353, mai 2011, doi: 10.1016/j.jsv.2010.11.018.
- [6] S. C. Stanton, C. C. McGehee, et B. P. Mann, « Nonlinear dynamics for broadband energy harvesting: Investigation of a bistable piezoelectric inertial generator », *Physica D: Nonlinear Phenomena*, vol. 239, n° 10, p. 640-653, mai 2010, doi: 10.1016/j.physd.2010.01.019.
- [7] A. J. Sneller, P. Cette, et B. P. Mann, « Experimental investigation of a post-buckled piezoelectric beam with an attached central mass used to harvest energy », *Proceedings of the Institution of Mechanical Engineers, Part I: Journal of Systems and Control Engineering*, vol. 225, n° 4, p. 497-509, juin 2011, doi: 10.1177/0959651811401954.
- [8] W. Q. Liu, A. Badel, F. Formosa, Y. P. Wu, et A. Agbossou, « Novel piezoelectric bistable oscillator architecture for wideband vibration energy harvesting », *Smart Mater. Struct.*, vol. 22, n° 3, p. 035013, mars 2013, doi: 10.1088/0964-1726/22/3/035013.
- [9] C. Saint-Martin, A. Morel, L. Charleux, E. Roux, A. Benhemou, et A. Badel, « Power expectation as a unified metric for the evaluation of vibration energy harvesters », *Mechanical Systems and Signal Processing*, vol. 181, p. 109482, déc. 2022, doi: 10.1016/j.ymsp.2022.109482.
- [10] A. Morel, A. Badel, R. Grézaud, P. Gasnier, G. Despesse and G. Pillonnet, « Resistive and reactive loads' influences on highly coupled piezoelectric generators for wideband vibrations energy harvesting », *Journal of Intelligent Material Systems and Structures*, vol. 30, n° 3, p. 386-399, févr. 2019, doi: 10.1177/1045389X18810802.
- [11] Y. Liao et J. Liang, « Maximum power, optimal load, and impedance analysis of piezoelectric vibration energy harvesters », *Smart Mater. Struct.*, vol. 27, n° 7, p. 075053, juill. 2018, doi: 10.1088/1361-665X/aaca56.
- [12] C. Lan, Y. Liao, G. Hu and L. Tang, « Equivalent impedance and power analysis of monostable piezoelectric energy harvesters », *Journal of Intelligent Material Systems and Structures*, vol. 31, n° 14, p. 1697-1715, août 2020, doi: 10.1177/1045389X20930080.
- [13] S. Bae et P. Kim, « Load Resistance Optimization of a Broadband Bistable Piezoelectric Energy Harvester for Primary Harmonic and Subharmonic Behaviors », *Sustainability*, vol. 13, n° 5, p. 2865, mars 2021, doi: 10.3390/su13052865.
- [14] T. Huguet, A. Badel, et M. Lallart, « Parametric analysis for optimized piezoelectric bistable vibration energy harvesters », *Smart Mater. Struct.*, vol. 28, n° 11, p. 115009, nov. 2019, doi: 10.1088/1361-665X/ab45c6.
- [15] R. L. Harné, M. Thota, et K. W. Wang, « Concise and high-fidelity predictive criteria for maximizing performance and robustness of bistable energy harvesters », *Appl. Phys. Lett.*, vol. 102, n° 5, p. 053903, févr. 2013, doi: 10.1063/1.4790381.